https://doi.org/10.48048/tis.2025.9286

The Influence of Reactant Concentration on the Characteristics of the As-Synthesized Cryptomelane Nanoparticles Prepared using Precipitation Method and Its Catalytic Performance for the Degradation of A Dye

Amir Awaluddin[1,*], Aulia Nur Ilahi[1], Erwin Amiruddin[2], Siti Saidah Siregar[1] and Zidna Mahira Milla[1]

[1]*Department of Chemistry, Riau University, Pekanbaru, Indonesia*
[2]*Department of Physic, Riau University, Pekanbaru, Indonesia*

([*]Corresponding author's e-mail: amir.awaluddin@lecturer.unri.ac.id)

Received: 7 November 2024, Revised: 28 December 2024, Accepted: 4 January 2025, Published: 28 February 2025

Abstract

The high purity of the nanostructured cryptomelane-type manganese oxide catalysts was successfully synthesized using the different ratio concentrations of $KMnO_4$ over glucose through a co-precipitation method. The both reactants were simultaneously mixed with the ratios of $KMnO_4$ to glucose of 0.4M/0.6M, 0.2M/0.3M, 0.08M/0.12M and 0.04M/0.06M, respectively. The average oxidation states (AOS) Mn of the products were determined using the back-titration method, whereas the crystalite size was calculated using Scherrer equation. The XRD analysis showed that while the phase structure remained unaffected by the concentration and calcination temperature, it had a notable impact on AOS of Mn, the morphology and the particle size as shown by the SEM images. The lowest concentration ratio resulted in the small particle size and the low AOS of Mn of the as-synthesized cryptomelane, which correlated with more Mn^{3+} concentration or oxygen defect in the as-synthesized cryptomelane. The vibrational mode Mn-O was demonstrated by the absorption bands appearing in the FTIR characterization results. The specific Mn-O vibrations of the cryptomelane were demonstrated using Raman spectroscopy. The catalytic activity of the as-synthesized catalysts was tested in its ability to degrade MB using a Fenton-like method. The results indicated that there is a strong correlation between the catalytic performance and Mn^{3+} concentration or oxygen defects present in the catalyst. The catalyst with the lowest concentration ratio possessing the high Mn^{3+} concentration or oxygen defects demonstrated better catalytic activity compared to the other as-synthesized catalysts. The optimization of the catalyst was performed by varying solution pH, H_2O_2 volume, catalyst mass, and initial concentration of methylene blue (MB). According to the research findings, this catalyst achieved a MB degradation rate of 97.01 ± 0.33 % after 120 min of contact time. This result was obtained under conditions of pH = 11, with 15 mL of 30 % H_2O_2, a catalyst mass of 50 mg and an initial MB concentration of 30 ppm.

Keywords: Cryptomelane nanoparticles, Co-precipitation method, Fenton-like process, Methylene blue

Introduction

Manganese oxides have been used in the various applications due to its unique structure and properties, its mixed valence of manganese (Mn^{2+}, Mn^{3+} and Mn^{4+}), strong oxidizing agent characteristics, good adsorption ability, wide availability in nature, low band gap, low-cost synthesis, and environmental friendliness [1]. Some reports suggested that manganese oxides can serve as a highly active heterogeneous Fenton catalyst for removing dyes from water and wastewater [2,3]. Manganese oxide exhibits different structures such as layers or tunnels, depending on the arrangement of the unit structure (MnO_6) and the synthesis method [4].

Manganese oxides like birnessite and cryptomelane have been successfully synthesized using the sol-gel method from $KMnO_4$ and glucose by adjusting the reactant concentrations. The varying the

concentration ratios of $KMnO_4$ and glucose resulted in the different phase manganese oxide products. For instance, the birnessite was produced with the high concentrations of $KMnO_4$/glucose (0.16M/0.23M), while the lower concentrations yield manganese oxide cryptomelane/Mn_2O_3 (0.06M/0.09M) and Mn_2O_3 (0.03M/0.05M) [5]. also conducted synthesis with a fixed $KMnO_4$ concentration (0.27M) but varied the glucose concentration, producing birnessite at high glucose concentrations (0.4M and 0.2M), cryptomelane at lower concentrations (0.10M), and amorphous MnO_x at the lowest concentration (0.05M). Additionally, the sol-gel method has been utilized for cryptomelane-type manganese oxide [6] as well as for manganosite-type manganese oxide [7]. Cryptomelane has shown excellent catalytic activity in degrading MB [8]. The birnessite successfully converted into cryptomelane using a precipitation method with $KMnO_4$ and reductant $H_2C_2O_4$ [9], maltose [10] with different modes of the addition of $KMnO_4$ and reductans. The manganese oxide successfully synthesized via a precipitation method with $KMnO_4$ and $H_2C_2O_4$ for MB degradation, achieving a degradation percentage of 97.73 % [11]. The manganese oxide was also successfully synthesised from $KMnO_4$ and glucose using the model B precipitation method conducted by Subramanian *et al.* [9], for the degradation of MB with a percent degradation reaching 91.00 % [12]. The synthesis of cryptomelane using a precipitation method with simultaneous variations in $KMnO_4$ and glucose reactant concentrations has not been previously reported.

The textile industries are expanding in response to the growth of world population, textile and textile-related industries. However, challenges arise when textile industrial wastes, particularly liquid dye wastes, are improperly managed and discharged into water bodies, leading to environmental impacts [13]. The dye commonly used in the textile industry is MB [14]. MB has a heterocyclic aromatic structure and is frequently employed to color leather, silk, plastic, paper, and paint. Pollution of water by MB can lead to a decrease in dissolved oxygen content, impacting photosynthetic activity and disrupting the aquatic ecosystem [15]. According to Fathoni [16], MB is toxic and can pose health risks to humans. Acute exposure to MB in humans can result in increased heart rate, vomiting, and cyanosis [17]. The maximum allowable concentration of MB, as per the Decree of the Minister of the Environment (Kep-51/MENLH/10/1995), is 5-10 mg/L. Therefore, it is essential to conduct studies on effective removal of MB from polluted water.

Various methods have been employed to treat wastewater containing MB, including electrocoagulation techniques [18] adsorption using fly ash [19], chemical oxidation using composites [20], and photocatalysts. Among these methods, the adsorption method is a common, simple, efficient, and cost-effective approach [21]. However, the adsorption method only transfers pollutants to the adsorbent, which can be problematic if the adsorbent is not reusable. Advanced Oxidation Processes (AOPs) show promise in wastewater treatment due to their high efficiency in removing refractory compounds [22]. AOPs involve oxidation processes that generate hydroxyl radicals (OH•) primarily for the destruction of contaminants in wastewater. Hydroxyl radicals oxidize pollutants into non-toxic products, such as carbon dioxide (CO_2) and water (H_2O). The Fenton method, a type of AOP, utilizes iron metal to activate H_2O_2 and produce hydroxyl radicals [23]. Manganese oxide is commonly used as a catalyst in the Fenton method due to its environmental friendliness, affordability, and high catalytic activity in degrading organic compounds [24].

In this study, the cryptomelane-type manganese oxides were synthesized using the precipitation method by mixing the $KMnO_4$ and glucose simultaneously while varying the reactant concentrations. The cryptomelanes were subsequently evaluated as catalysts for the degradation of MB using a Fenton-like process. The effects of the type of catalysts, solution pH, initial MB concentration, hydrogen peroxide (H_2O_2) volume, and catalyst mass were optimized to achieve maximal degradation of MB.

Materials and methods

Materials

The materials used in this study are potassium permanganate ($KMnO_4$) (Merck), glucose ($C_6H_{12}O_6$. H_2O) (Merck), hydrogen peroxide (H_2O_2), MB (Merck), Whatman No. 42 filter paper, aluminum foil, aqua DM, and low-lint tissue (chemical grade).

Synthesis of catalyst

The synthesis of the manganese oxide catalyst was carried out with a mole ratio of $KMnO_4$: Glucose of 2:3 (0.02 mol: 0.03 mol) using the precipitation method Subramanian *et al.* [9] with variations in the concentration of $KMnO_4$ /Glucose reactants: 0.4/0.6 M; 0.2/0.3 M; 0.08/0.12 M; 0.04/0.06 M. The catalysts are then abbreviated as catalysts C-1, C-2, C-3, and C-4, respectively. For the C-1 catalyst, 3.16 g of $KMnO_4$ was dissolved in 50 mL of aqua DM, whereas 5.4 g of glucose was also dissolved in 50 mL of aqua DM. Both solutions were then mixed together in a glass beaker and then stirred using a magnetic stirrer at 300 rpm for 30 min. The solution was then heated up to 60 °C and stirred at 300 rpm for another 30 min. The precipitate obtained was filtered using Whatman No. 42 filter paper and dried using an oven at 120 °C for 4 h. Furthermore, the solid was calcined at 700 °C for 4 h which will then be characterized and applied to MB dye. The catalysts C-2, C-3 and C-4 were prepared on the same ways, but using the different amount of aqua DM.

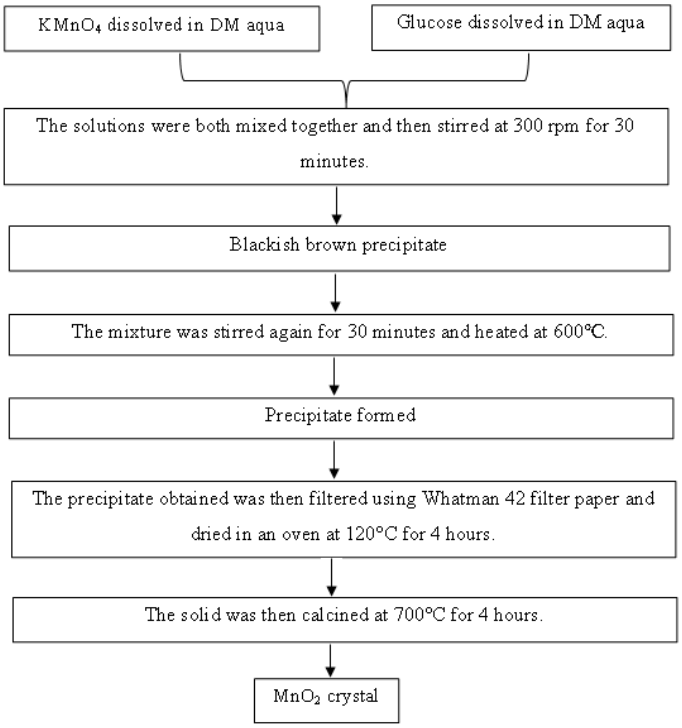

Figure 1 Schematic diagram of the catalyst synthesis.

Characterization of catalyst

The characterization of the as-synthesized manganese oxides was conducted using X-Ray Diffraction (XRD), Fourier Transform Infrared Spectroscopy (FTIR), Raman spectroscopy and Scanning Electron Microscopy (SEM). The AOS of the as-synthesized were carried out by the back-titration method by Ciu *et al.* [47]. The crystallite sizes of the samples were calculated using Scherrer equation. For AOS Mn determination, about 0.05 g of sample was dissolved into 5 mL of oxalic acid solution ($H_2C_2O_4$) 0.5 M and 5mL of sulfuric acid solution (H_2SO_4) 0.5 M. The mixture was then heated up to 60 °C until the all solids were dissolved. The mixture was then transferred into a 250 mL Erlenmeyer and titrated using 0.02 M potassium permanganate ($KMnO_4$) solution until a color change occurred from colorless to mauve pink.

Catalyst activity test

MB 50 ppm solution as much as 25 mL was taken and 60 mL of aqua DM was put into a glass container. 50 mg of C-1 catalyst was weighed and added to the solution. The solution was stirred using a magnetic stirrer at 400 rpm for 30 min. Then, 15 mL of 30 % H_2O_2 solution was added to the solution. A solution of 10 mL

was taken at 10, 20, 30, 40, 50, 60, 90 and 120 min and put into a test tube and then centrifuged at 3,000 rpm for 15 min to separate the manganese oxide catalyst from the degraded MB solution. Next, the remaining MB concentration analysis was measured using a UV-Vis spectrophotometer at the optimum wavelength. The same procedure was carried out for the addition of catalysts C-2, C-3, and C-4.

Optimization of catalyst

MB solution of (50, 40, 30 ppm) as much as 25 mL was taken and aqua DM as much as (55, 60, 65, 70, 75 mL) was put into a glass jar then pH was adjusted at pH (2; 3; 5; 7.6; 8; 9; 11). Catalyst with the best degradation results (C-4 & C-4/500) as much as (0, 25, 50, 75 mg) was weighed and added to the solution. The solution was stirred using a magnetic stirrer at 400 rpm for 30 min. Then, 30 % H_2O_2 solution as much as (0, 5, 10, 15, 20 mL) was added to the solution. A solution of 10 mL was taken at 10, 20, 30, 40, 50, 60, 90 and 120 min and put into a test tube and then centrifuged at 3,000 rpm for 15 min to separate the manganese oxide catalyst from the degraded MB solution. Furthermore, the remaining MB concentration analysis was measured using a UV-Vis spectrophotometer at the optimum wavelength.

Results and discussion

Characterization of catalysts

The as-synthesized catalysts were first characterized using XRD to determine the crystal structure, crystal size, and percent crystallinity. **Figure 2** displayed the diffractogram of the as-synthesized catalyst at the different concentration ratios and different calcination temperatures. All peaks were matched to the standard JCPDS No. 10.00946214 of cryptomelane diffraction pattern. The catalyst C-1 exhibited 8 peaks at 2θ of 13.04, 18.34, 28.93, 37.69, 42.13, 49.94, 60.34 and 69.65 ° with reflection planes (101), (002), (103), (112), (013), (114), (215), and (604), respectively. The catalyst C-2 showed the similar peaks as the C-1 with the additional 1 peak at 36.34 ° due to (400) reflection plane. The catalyst C-3 displayed only 6 peaks due to the missing peaks at 42.13 and 69.65 ° with reflection plane (604) and (013). The catalyst C-4 also exhibited 6 peaks due to the missing 2 peak at 49.94 and 32.62 °. The calcination temperatures seem to have a minor effect on the as-synthesized manganese oxides as shown in **Figure 2(b)**.

All the peaks observed in the 4 catalysts corresponded to the cryptomelane type manganese oxide. The characteristic peaks of cryptomelane at 28, 37 and 60 ° are clearly visible in the diffractograms of the 4 catalysts with relatively high intensity. Similar results were also reported by Asleni *et al.* [12] who produced the cryptomelane-type manganese oxide after calcination at 600 °C for 4 h with a reactant molar ratio of 2:3.

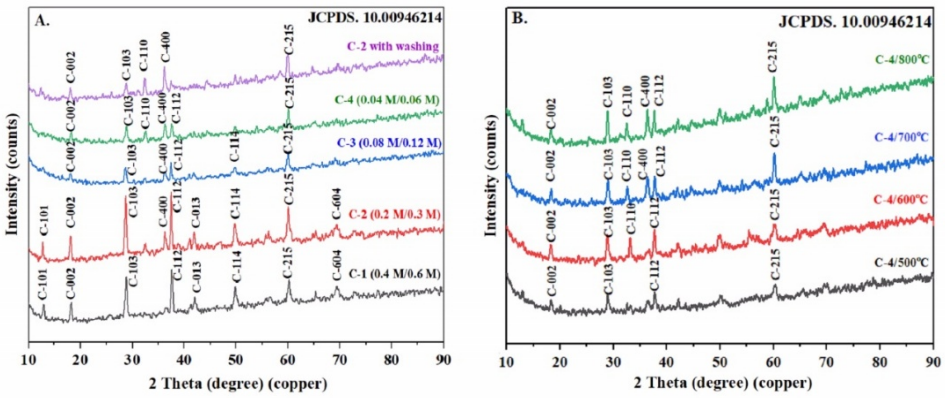

Figure 2 The XRD patterns of as-synthesized cryptomelane catalyst at (a) different concentration ratio of reactans at 700 °C and (b) different calcination temperatures with ratio $KMnO_4$/glucose = 0.04M/0.06M. Description C = cryptomelane.

The **Figure 2(a)** clearly showed that while the reactant concentration ratio did not alter the crystal phase, it significantly impacts the intensity of the observed peak. This was contradicted with the results

reported [5]. Ching *et al.* [5] synthesized the manganese oxides with the different concentration ratios of $KMnO_4$ over glucose, but used sol-gel method. The high concentration reactant resulted in the layer birnessite-type manganese oxide, while the low concentration of reactant led to the formation of mixture phase cryptomelane and Mn_2O_3. The cryptomelane phase was obtained with the moderate reactant concentration. Subramaniam ref synthesized manganese oxides using a precipitation method, employing a similar approach of adding reactants with current study and the fixed reactant concentration, but with significantly lower reactant concentration. The synthesis resulted in the formation of the birnessite or cryptomelane, depending upon the calcination temperature and reaction time. The birnessite phase was obtained in the low calcination temperature (400 °C) and short reaction time (2 h), whereas the cryptomelane started to appear at the similar calcination temperature with longer reaction time (4 h). The increase in temperature up to 600 °C led to the formation of the cryptomelane with greater intensity. In our study shown in **Figure 2(b)**, the calcination temperature from 500 to 800 °C seems to have no effect to the phase change. All the above data suggested that the cryptomelane is more thermodynamically stable phase than birnessite. This is consistent with previous study [8,9,11] where thermal stability of cryptomelane is higher than that of birnessite. Yu *et al.* [25] also synthesized birnessite and cryptomelane using $KMnO_4$ and glucose by adding the glucose solution into the $KMnO_4$ solution dropwise. Either the birnessite or cryptomelane phases were generated, it depended upon the washing process. The birnessite was obtained if the dried products were calcined up to 550 °C without washing process. If washed with water 3 times, the cryptomelane phase was generated with the calcination temperature similar to that of the birnessite. The author claimed that glucose content was responsible for the formation of the cryptomelane. A series of experiments with the different molar ratios of $KMnO_4$ to glucose and washing and without washing process were conducted to support the claim. In contrast, the current results indicated that the washing processes seem to have the no effect on the crystal phase of manganese oxides. The dried samples with or without washing process always produced the cryptomelane as shown in the XRD pattern in **Figure 2**. Becerra *et al.* [26] synthesized manganese oxides from reduction of $KMnO_4$ using solid-state reaction by varying the synthesis temperature. The birnessite-type manganeses oxides were produced at 400 and 800 °C even at the different heating rate. Another solid-state method was used by Saidah [7] to synthesize manganese oxide using redox reaction between $KMnO_4$ and glucose with difference of mole ratios, calcination temperatures and calcination time. The products were birnessite-type manganese oxides differed only in crystallinity and purity even with or without washing process. Ghaly [28] synthesized cryptomelane through oxidation method by oxidizing the acidified $MnSO_4$ with permanganate solution. With this method, the nano-cryptomelane was obtained, which was confirmed by Raman spectroscopy. Zhou *et al.* [29] synthesized the pure cryptomelane nanowires by the hydrothermal redox reaction of $KMnO_4$ and $(NH_4)_2C_2O_4 \cdot H_2O$. Nguyen *et al.* [30] used a novel pathway to synthesize cryptomelane nanosheets from birnessite via tuning pH and molar ratio of $KMnO_4$ and oxalic acid. These findings indicated that various synthesis methods and post-synthesis treatments frequently led to different crystal structures.

XRD data can also be used to determine the average crystalite size. Data from **Table 1** indicated that the reactant concentration play significant role in the crystalite size and AOS Mn of the as-synthesized cryptomelane. Higher reactant concentrations resulted in smaller crystalite sizes and AOS of Mn (**Table 1**). At higher reactant concentrations, collisions become more frequent, which speeds up the reaction. This increased frequency of collisions and promoted nucleation and particle formation. At low reactant concentrations, however, the larger crystalite size was obtained. Similar results were also reported by previous study [5].

The average crystalite sizes of the produced catalysts were determined by Debye-Scherrer equation:

$$D = \frac{0.941\,\lambda}{\beta \cos \theta} \quad (1)$$

where D is crystal size (nm), λ is the wavelength of X-ray (0.15406 Å) and β is Full Width Half Maximum (FWHM) (radian).

Table 1 also displayed the AOS of the as-synthesized catalysts, which were calculated by the

permanganate-oxalic acid back titration method with the following equation:

$$M_2 = \frac{2\,V1M1}{5V2} \quad (2)$$

where M_2 is $KMnO_4$ concentration, V_1 and M_1 is volume and concentration of oxalic acid and V_1 is volume of $KMnO_4$.

Table 1 Average crystalite size and AOS of of the synthesized catalyst.

	Catalysts						
Average crystalite size (nm)	C-1	C-2	C-3	C-4/700	C-4/500	C-4/600	C-4/800
	14.30	17.16	19.81	20.89	73.34	30.21	60.76
AOS of Mn	4.08	4.01	3.81	3.79	3.78	3.78	3.84

AOS = Average oxidation state.

The as-synthesized catalysts were characterized using FTIR to determine the lattice vibration. **Figure 3** showed the FTIR spectra (normalized) of the catalysts as synthesized. Mn-O vibrations appeared in the wavenumber range of 400 - 700 cm^{-1}. According to Stella *et al.* [31] Mn-O bending vibrations are observed in the lower wavenumber region, whereas Mn-O stretching vibrations are found in the higher wavenumber region. The IR spectra of Mn-O bending vibrations from this study appear in the absorption bands 431, 432, 433, 435 and 445 cm^{-1}. Meanwhile, Mn-O stretching vibrations appear in the absorption bands 527, 532, 539, 594, 668 and 682 cm^{-1}. The O-Mn-O vibrations from the C-2 and C-4 catalysts are also observed at wavenumbers 482 and 488 cm^{-1}. To confirm the Mn-O vibrations are due to a cryptomelane-type manganese oxide, the Raman spectroscopy were conducted and the results are shown in **Figure 4**. It is difficult to differentiate Mn-O vibrations in layered manganese oxide (birnessite) and manganese oxide with a tunnel structure (cryptomelane) [32].

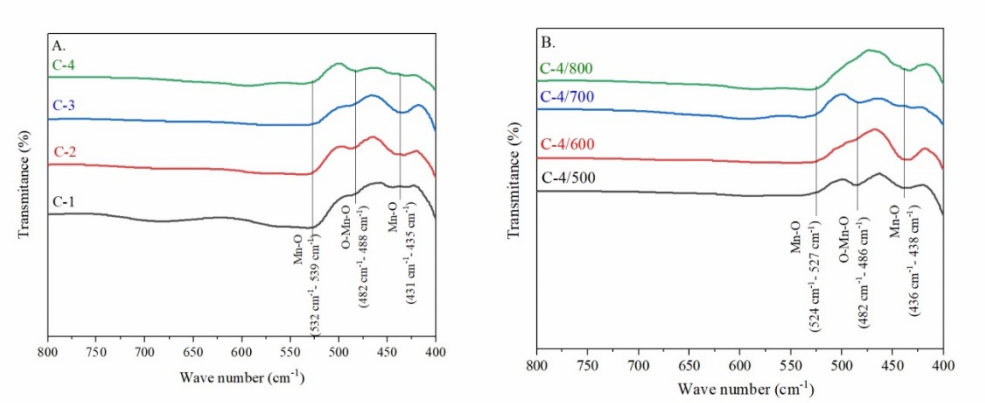

Figure 3 The IR spectra of as-synthesized cryptomelane catalyst at (a) different concentration reactant at 0.04/0.06, 0.08/0.12, 0.2/0.3, 0.4/0.6 M and (b) different temperatures from 500 to 800 °C.

The selected Raman spectra for the C-4/ 500 and C-4/700 samples prepared with the molar ratio $KMnO_4$/glucose of 0.04/0.06 M and calcinet at 500 and 700 °C were shown in **Figure 4**. The Raman spectra for the specific vibration of the Mn-O were observed at Raman shifts of 184, 579 and 656 cm^{-1}. According to Hou *et al.* [33], the strong peak appeared at the 655 cm^{-1} absorption band is due to the symmetric stretching vibration of Mn-O, which is perpendicular to the direction of the octahedral double chain MnO_6, and the weak peak found at the 576 cm^{-1} corresponds to the displacement of oxygen atoms relative to manganese atoms along the octahedral chain. The results from Hou *et al.* [33] was in good agreement with those from this

study, showing peaks at 654 and 579 cm^{-1}. Jakubek *et al.* [34] also reported similar findings, identifying characteristic absorption bands for cryptomelane at 577 and 632 cm^{-1}, which correspond to Mn-O vibrations. Additionally, the peak observed at 184 cm^{-1} was linked to the translational motion of octahedral MnO_6 units [28].

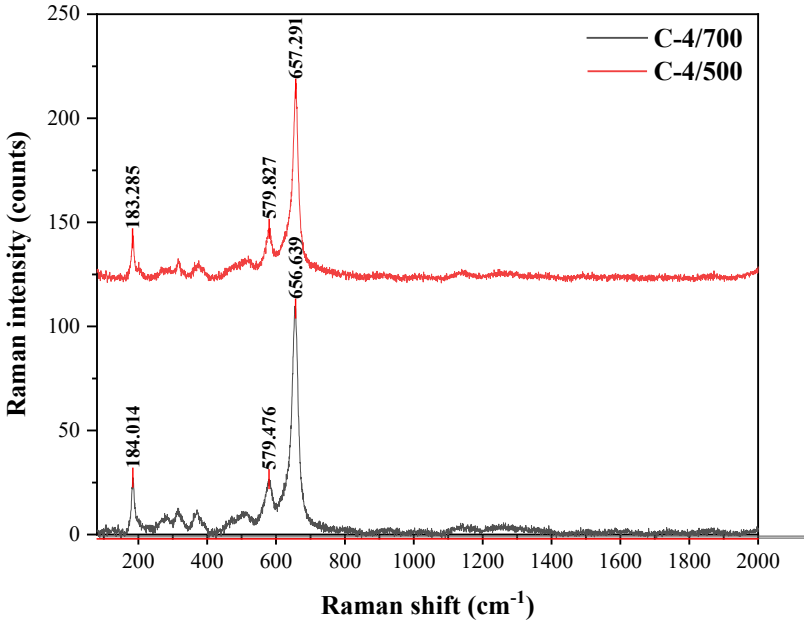

Figure 4 The Raman spectra of as-synthesized cryptomelane catalyst C-4 at 500 and 700 °C.

The AOS of manganese Mn in the as-synthesized cryptomelane-type manganese oxides was determined by an oxalic acid-permanganate back titration method. The results of the AOS Mn in the samples were seen in **Table 1**. **Table 1** shows that both the molar ratio of $KMnO_4$ to glucose and the calcination temperature significantly impact the AOS of the synthesized cryptomelane. A higher molar ratio of $KMnO_4$ to glucose resulted in a higher AOS value and a higher calcination temperature also resulted in a higher AOS value. A low AOS value suggests a high concentration of Mn^{3+} ions in the MnO_2. The presence of Mn^{3+} or oxygen vacancy is likely to be associated with defects in the MnO_2 structure as revealed by Awaluddin *et al.* A defect concentrations in MnO_2 have been reported to have a significant role for a catalytic reaction [34-36]. The results showed that β-MnO_2 (pyrolusite) exhibits the highest AOS, α-MnO_2 (cryptomelane) has a moderate AOS, and δ-MnO_2 (birnessite) displays the lowest AOS. Mn^{3+} is known to be crucial for the catalytic reactivity of Mn-based catalysts [34]. Specifically, Mn^{3+} exhibits longer (Jahn-Teller distorted) and thus weaker Mn-O bonds compared to Mn^{4+}, which leads to enhanced catalytic activity in water oxidation [35,36].

Table 2 The Selected data for C-1 and C-4 samples analyzed by gas surface area (GSA).

Catalysts	Surface area BET (m^2/g)	Surface area BJH (m^2/g)	Pore volume (cc/g)	Total pore volume (cc/g)	Pore radius (Å)	Average pore radius (Å)
C-1	2.272	1.255	0.006	0.00625	89.157	55.0283
C-4/700 °C	1.599	1.228	0.005	0.004961	34.322	62.0548
C-4/500 °C	2.930	2.209	0.012	0.01075	155.194	73.4068

The GSA data presented in **Table 2** shows that the calcination temperature have a considerable impact on the surface area, pore volume and pore radius, whereas the concentration has a smaller impact than that of calcination temperature. According to the table, the sample C-1/700 prepared from the most concentrated solution ratio has larger total surface area, pore volume and pore radius compared to the sample C-4/700. The data also shows that catalyst C-4/500 has higher BET surface area and adsorption capacity compared to catalyst C-4/700. This observation is in accordance with the data from the AOS measurements, the higher temperatures lead to the higher AOS values (fewer defects). These results are also in agreement with the work of Subramanian *et al.* [9], which indicated that high calcination temperatures can cause sintering and phase transitions, resulting in the closure of some pores. The high BET surface area possessed by the C-1/700 catalyst does not increase its catalytic activity. This is due to the fact that nitrogen molecules used in BET surface area determination have smaller size than molecule of MB. The number of N_2 molecules that can be absorbed in the catalyst pore will certainly be more than MB molecules [37]. Thus, the high surface area does not necessarily reflect the ability of the catalyst to degrade MB.

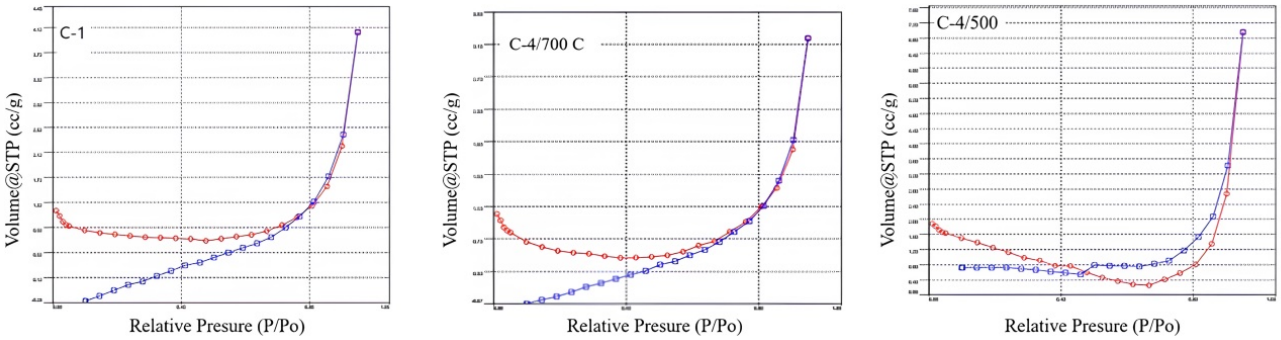

Figure 5 The Nitrogen adsorption-desorption isotherms of C-1/700, C-4/500 and C-4/700 shows BJH pore size. Description: Adsorption (blue line) and desorption (red line).

The **Figure 5** shows that the C-1 catalyst exhibits a type 5 isotherm, while the C-4/500 and C-4/700 catalysts display a type IV isotherm, characteristic of mesoporous materials. This type IV isotherm finding aligns with prior studies by Subramanian *et al.* [9]. The C-4/500 and C-4/700 catalysts demonstrate a strong adsorption capability right from the start, while the C-1/700 catalyst exhibits a slower initial adsorption rate, which only improves after some time. The surface of a particular catalyst can be seen from the results of analysis using SEM-EDX. **Figure 6** shows that the black part shows the porosity while the white part represents the solid surface. The SEM images at 15,000x magnification show that the C-4/700 °C catalyst produces a more homogeneous and small particle size with a particle length of ± 50 nm when compared to the C-1/700 °C catalyst which is ± 90 nm. The C-4/700 catalyst generates more porosity compared to the other catalysts. This occurs because the introduction of a low reactant concentration slows down the nucleation process and particle growth. As a result, there is less nucleation at the start of the reaction, allowing for more stable and uniform particle growth. Furthermore, the low concentration reduces the aggregation rate [38,39]. It also indicates that the particles on the C-4/500 °C catalyst are clustered together, which can influence both the particle size and the distribution of particle sizes [40]. Therefore, the catalyst synthesized at 500 °C promotes more agglomeration compared to those prepared at 700 °C. This finding aligns with earlier studies [41] indicating that higher temperatures lead to a reduction in agglomerates, as noted by other researchers as well [42].

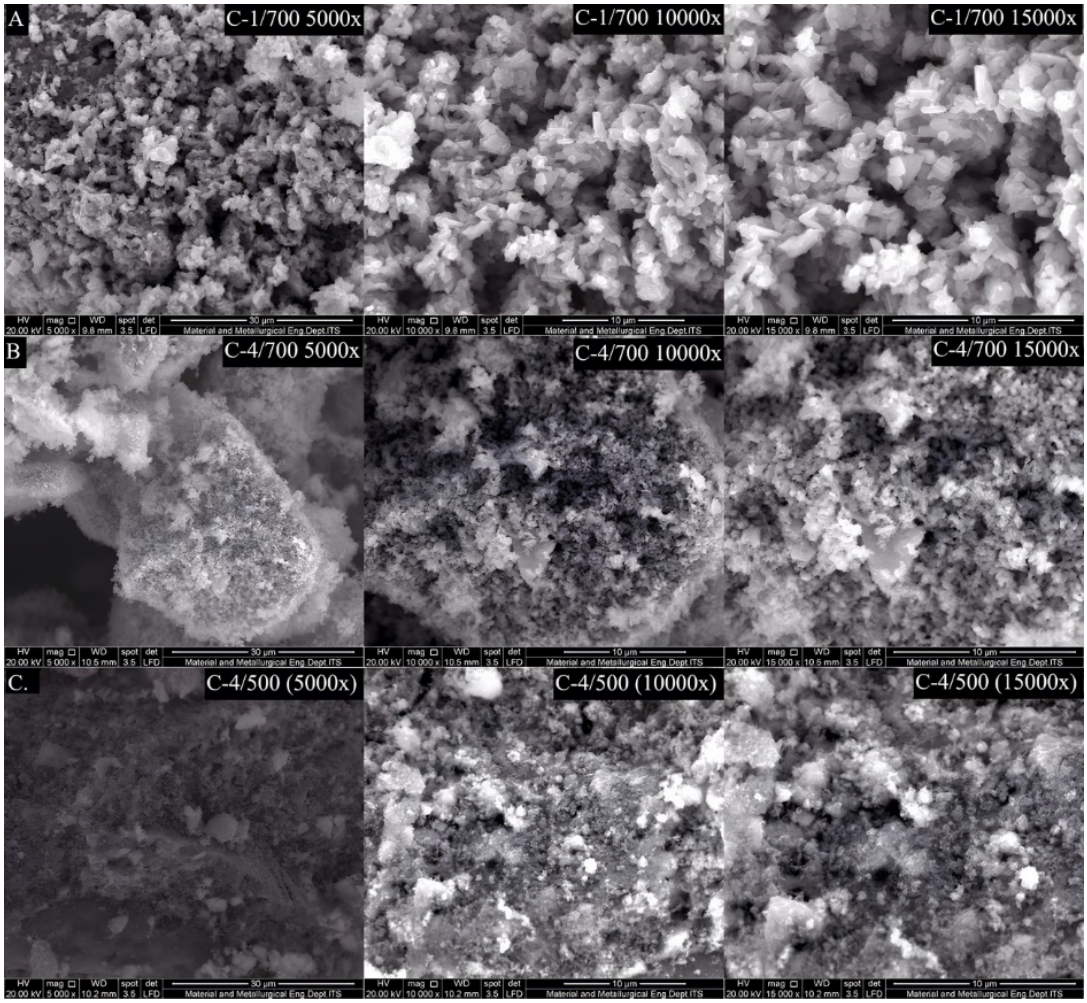

Figure 6 The SEM of selected catalysts as synthesized catalyst (a) C-1/700 °C (b) C-4/700 °C, and (c) C-4/500 °C at magnifications of 5000x, 10000x and 15000x.

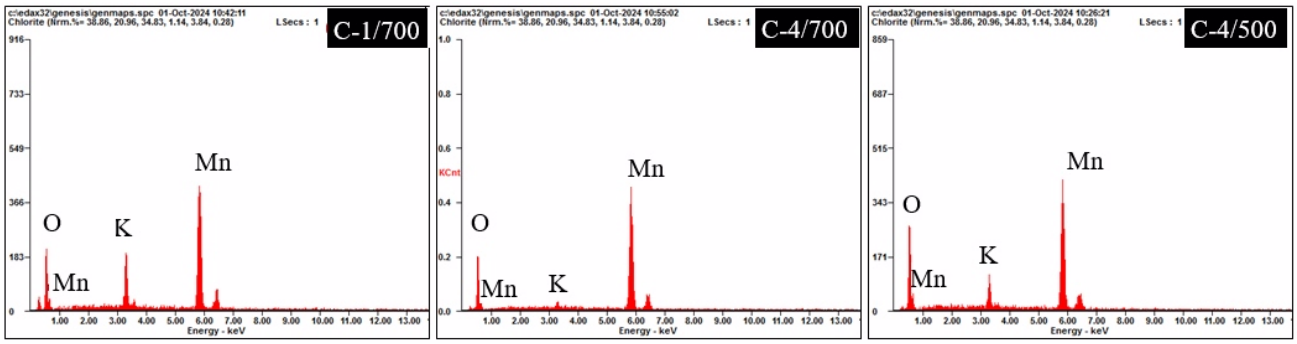

Figure 7 The selected EDX data for catalysts: C-1/700, C-4/700, and C-4/500 °C.

The **Figure 7** and **Table 3** display the EDX data for C-1/700, C-4/700, and C-4/500 °C catalysts. Based on the EDX results, the percentage of O atoms decreased as the concentration decreased, indicating the occurrence of OVD. The results revealed that the C-4/700 °C catalyst possesses the lowest oxygen content, indicating more oxygen vacancies are available as active sites for the catalytic reaction. Oxygen Vacancy Defect (OVD) affect the ratio of Mn and O content but can increase the catalytic activity of the catalyst as reported by previous studies [43,44].

Table 3 The EDX data for the selected catalysts.

Catalyst	Weight %			Atomic%		
	O K	**K K**	**Mn K**	**O K**	**K K**	**Mn K**
C-1/700 °C	17.37	10.67	71.96	40.69	10.22	49.09
C-4/700 °C	14.73	01.58	83.69	37.05	01.62	61.32
C-4/500 °C	20.61	05.86	73.53	46.40	05.40	48.20

The catalytic studies of as-synthesized catalyst

The catalytic performance of the as-synthesized catalysts was evaluated based on their ability to degrade MB using a Fenton-like process. The Catalysts C-1, C-2, C-3, and C-4 were all tested under identical conditions: 25 mL of 50 ppm MB solution, 65 mL of distilled water, 15 mL of 30 % hydrogen peroxide, 50 mg of catalyst and no pH adjustment. The influence of the type of catalyst prepared at different reactant concentration on MB degradation at the different reaction time is illustrated in **Figure 8(a)**. The results indicated that the concentration of reactan affects catalytic performance, as confirmed by the ANOVA test detailed in Appendix 13, which shows significant differences in degradation percentages among the different catalysts. After 120 min, the degradation percentages for C-1, C-2, C-3 and C-4 were 61.03 ± 0.60 %, 66.51 ± 0.50 %, 68.25 ± 1.09 % and 73.98 ± 0.33 %, respectively. Percent degradation was calculated using the following Eq. (3):

$$\frac{C0-C}{C0}\,100\ \% \qquad (3)$$

where C_0 is the initial concentration of MB solution before degradation and C is the concentration of MB solution at a certain min. The degradation graph was processed using the C/C_0 value expressing the normalized MB solution concentration as the Y-axis versus time (min) as the X-axis.

The data from crystalite sizes seems to contradict with the degradation of MB. Although the catalyst C-4 has the largest crystalite size, it exhibits the highest catalytic performance, contrary to what would be expected. The degradation of MB was inversely related to the AOS Mn of the as-synthesized catalysts, meaning that lower AOS Mn levels led to greater MB degradation, as illustrated in **Table 1** and **Figure 8(a)**. A low value of AOS means more Mn^{3+} or oxygen vacancy presence in a material. The similar results were also reported by Awaluddin *et al.* [8]; the catalysts with low AOS Mn posseses high catalytic performance for the degradation of MB. Mn^{3+} is known to be crucial for the catalytic reactivity of Mn-based catalysts [16]. Specifically, Mn^{3+} exhibits longer (Jahn-Teller distorted) and thus weaker Mn-O bonds compared to Mn^{4+}, which leads to enhanced catalytic activity in water oxidation [35,36]. Hou *et al.* [33] suggested that Mn^{3+} arises due to the formation of OVD to maintain electrostatic balance. The presence of Mn^{3+} and OVD is described by Eq. (4) [33].

$$-Mn^{4+}\text{-}O^{2-}\text{-}Mn^{4+} \rightarrow -Mn^{3+}\text{-}\Upsilon\text{-}Mn^{3+}\text{-}+ \tfrac{1}{2}\ O_2 \qquad (4)$$

According to Awaluddin *et al.* [8], Mn^{3+} ions belong to a d^4 system, with one electron in the highly reactive e_g^1 antibonding orbital. These highly reactive electrons in Mn^{3+} readily interact with hydrogen peroxide (H_2O_2), generating more hydroxyl radicals (OH•) and thereby enhancing the degradation of MB. The OVD plays a crucial role in the catalytic activity of metal oxides like manganese oxide, serving as an active site during the reaction. OVD induces lattice oxygen vacancies in the crystals [33]. A higher content of Mn^{3+} or more OVD leads to increased catalytic activity. These oxygen vacancies create reactive sites by facilitating interactions with surrounding molecules such as H_2O_2 and MB, due to the absence of oxygen making the area more accessible.

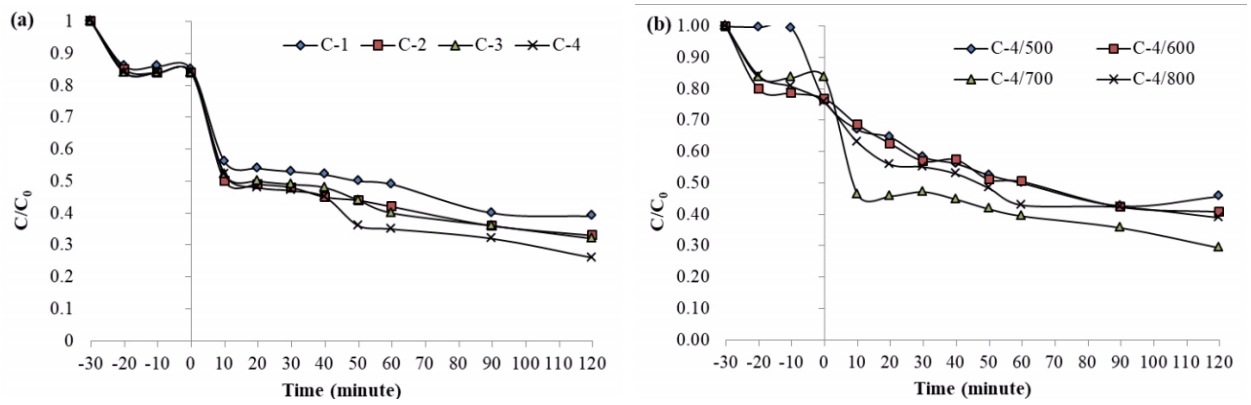

Figure 8 The effect of the type of catalyst on degradation of MB, the catalysts prepared at different molar ratios (a); the catalysts prepared at molar ratio $KMnO_4$/glucose of 0.04/0.06 at different calcination temperatures (b). Description: C_0 MB :12.5 ppm; volume of 30 % H_2O_2 :15 mL; mass of catalyst : 50 mg. C/C_0 = normalized concentration of MB.

The data from **Figure 8(a)** indicated that the C-4 catalyst posseses the best catalytic performance and thus was selected for studying how calcination temperature affects the degradation of MB. **Figure 8(b)** shows the effect of calcination temperature on the catalytic performance for the degradation of MB at different reaction time. It is obvious that the catalyst C-4/700 has the best catalytic performance, whereas the catalyst C-4/500 has the lowest catalytic performance. A higher temperature facilitates more reaction to occur since it posseses higher kinetic energy. The data from the average crystal size value shown in **Table 1** also supported this result, the catalyst C-4/700 with the highest catalytic performance also has the smallest average crystal size. There is also strong correlation between catalytic performance and the AOS value shown in **Table 1**. The C-4/700 catalyst with the low AOS value posseses the highest catalytic performance. The presence of more OVD in the C-4/700 catalyst could be responsible for the highest catalytic performance as reported by previous studies Hou *et al.* [33] Data from **Figure 8(b)**, however, revealed that the C-4/500 with similar AOS value to the C-4/700 has the low catalytic performance. Both catalysts were then tested to study the effect of solution pH on the degradation of MB.

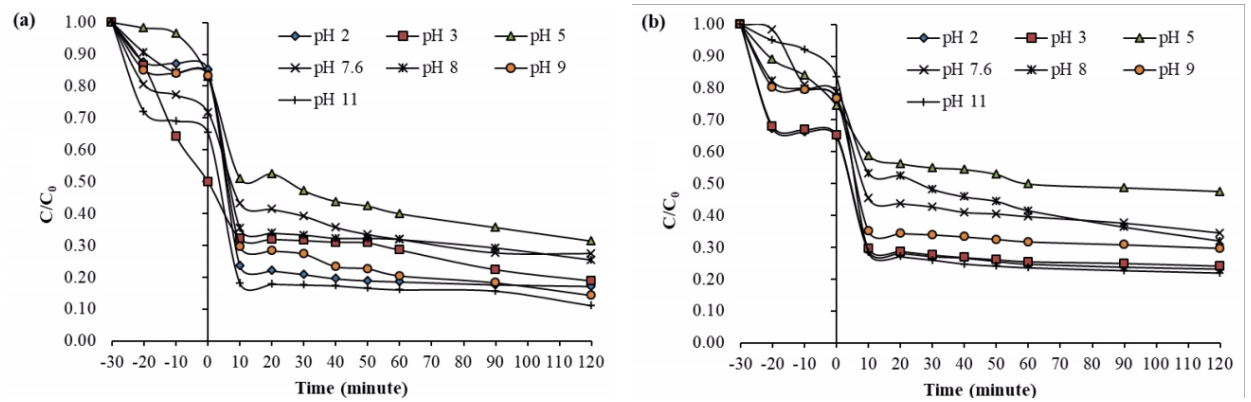

Figure 9 The effect of pH on the degradation of MB at different reaction time (a) The samples prepared at 700 °C (C-4/700) and (b) The samples prepared at 500 °C (C-4/500). Description: C_0 MB 12.5 ppm; volume of 30 % H_2O_2 15 mL; mass of catalyst 50 mg. C/C_0 = normalized concentration of MB.

The catalytic performance of the as-synthesized catalysts was evaluated across a range of pH values, including pH 2, 3, 5, 7.6, 8, 9 and 11. The effects of pH on the catalytic performance of the catalysts prepared at 500 °C (C-4/500) and 700 °C (C-4/700) are depicted in **Figures 9(a) - 9(b)**. An ANOVA test was performed to determine the impact of pH on the percent degradation of MB. The results indicated that pH significantly

influences MB degradation. The highest degradation rate, 88.97 ± 1.36 %, was observed at pH 11 after 120 min of reaction. Surprisingly, a high degradation rate of 82.89 ± 0.12 % was also recorded at pH 2 under the same reaction time. The catalysts maintained effective performance for MB degradation across other pH values as well, with the lowest degradation, 68.66 ± 2.83 %, occurring at pH 5. At basic pH, the catalyst's surface becomes negatively charged, enhancing electrostatic interactions with the positively charged MB molecules. This interaction promotes more reactions between MB molecules and the reactive species on the catalyst, leading to increased MB degradation. In this studies, H_2O_2 molecules were added to the reaction mixture to promote the production of hydroxyl radical (OH•). This reactive spesies then reacted with MB molecules to generate more simple molecules, or CO_2 gases and H_2O when complete oxidation occurred. The formation of the gases during the reaction was confirmed with the generation of bubbles following the reaction. Both **Figures 8** and **9** also displayed the removal of MB without the presence of H_2O_2 molecules. The values between –30 and 0 in the Y axis indicated the removal of MB without the addition of H_2O_2. The maximum of MB removal is about 30 % (**Figure 9(a)**), which could be due to an adsoption process. Following the addition of H_2O_2 , known as the Fenton-like method, the removal of MB continue to progress and achieve slow rate at 120 min of reaction time. This removal of MB was believed due to degradation process with OH• radicals acting as reactive species.

The reaction between H_2O_2 with metal oxides surfaces, generating OH radicals have been reported by previous reports [43]:

$$Mn^{4+} + H_2O_2 \rightarrow Mn^{4+}.H_2O_2 \quad (5)$$

$$Mn^{4+} + H_2O_2 \rightarrow Mn^{2+} + HO_2\bullet + H^+ \quad (6)$$

$$Mn^{2+} + H_2O_2 \rightarrow Mn^{4+} + OH\bullet + OH^- \quad (7)$$

$$HO_2\bullet \rightarrow H^+ + O_2\bullet^- \quad (8)$$

$$MnO_2.H_2O_2 \rightarrow HOO^- + H^+ \quad (9)$$

$$(HO\bullet, O_2\bullet^-) + MB\ (adsorbed) \rightarrow CO_2 + H_2O \quad (10)$$

$$2HO\bullet + 2HO\bullet \rightarrow O_2 + 2H_2O \quad (11)$$

Metal oxides have the ability to form reduction-oxidation pairs that can be used as catalysts in degrading organic compounds with the addition of H_2O_2 producing hydroxyl radicals (OH•) as strong oxidizing agents capable of degrading organic compounds [44]. The volume variation of 30 % H_2O_2 used in this study is (0, 5, 10, 15 and 20 mL). The effect of 30 % H_2O_2 volume on the percent degradation of MB can be seen in **Figure 10**. Anova testing data (Appendix 13) shows that the volume of H_2O_2 affects the percent degradation of MB.

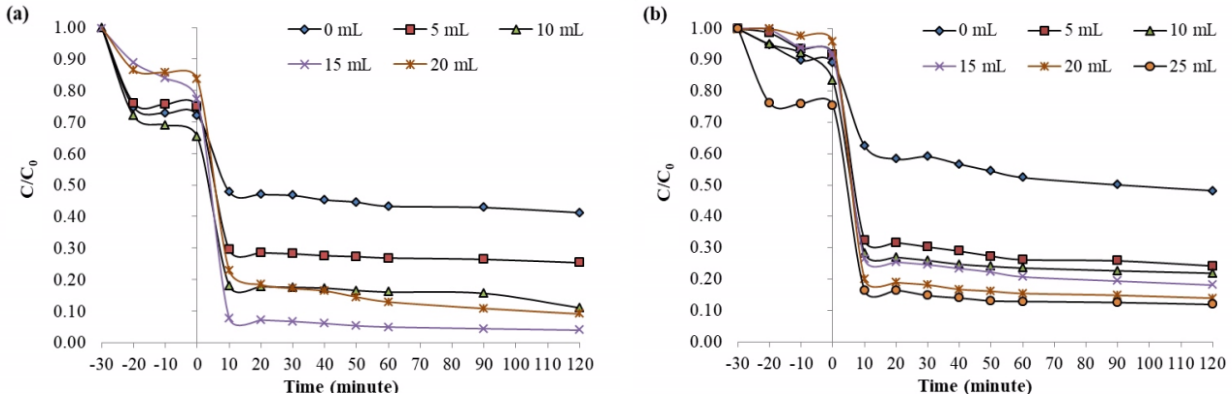

Figure 10 the curve of the relationship of time to C/C_0 ratio by the synthesized catalysts at different different volume H_2O_2 30 % by catalyst (a) C-4/700 and (b) C-4/500. Description: C_0 MB 12.5 ppm; pH 11; mass of catalyst 50 mg. C/C_0 = normalized concentration of MB.

It is obvious from the both **Figures 10(a) - 10(b)**. that the of H_2O_2 concentration had a sizable impact on the degradation of MB. Without the addition of H_2O_2 the maximum removal of MB was 58.75 ± 2.69 % for C-4/700 and 51.76 ± 7.11 % for C-4/500, respectively. For C-4/700 catayst, the addition of 5 mL of H_2O_2 increased the degradation of MB to 74.67 ± 1.42 %. When the volume of H_2O_2 was further increased to 15 mL, the degradation of MB rose to 96.07 ± 0.33 %. However, when the volume of H_2O_2 was increased to 20 mL, the degradation of MB dropped to 90.91 ± 0.43 %. This observation was also reported by previous studies (Merdoud *et al*. 2024). The C-4/500 also displayed a similar trend, but with lower catalytic performance. Without the addition of H_2O_2 , an adsorption process was believed to occur without degradation process. The positively charged MB particles would be adsorbed on the surface of the negatively charged C-4 catalyst at pH 11 and no degradation process occurs. The addition of H_2O_2 facilitated the generation of OH•, which then reacted with adsorbed MB molecule to produce simplier molecules or CO_2 and H_2O. The formation of OH• seems to be linear to the volume of 30 % H_2O_2 added, that is, the more the volume of is H_2O_2 added, the more OH- is produced. The results also indicated that there is a optimum volume of H_2O_2 for the maximum degradation of MB. The addition of 20 mL H_2O_2 caused the decreased degradation of MB.

According to Erda *et al.* [45], the addition of excess H_2O_2 volume causes the percent degradation to decrease as seen in Eqs. (11) - (13).

$$H_2O_2 + OH\bullet \rightarrow HO_2\bullet + H_2O \quad (12)$$

$$HO_2\bullet + OH\bullet \rightarrow H_2O + O_2 \quad (13)$$

$$OH\bullet + OH\bullet \rightarrow H_2O_2 \quad (14)$$

The accumulation of excess OH• due to excess H_2O_2 resulted in OH• reacting with H_2O_2 to produce HO_2• which is less reactive than OH• (Eq. (12)). Hydroxyl radicals could also react with HO_2• to produce water and oxygen which can be shown by Eq. (13). In addition, OH• could react with OH- to produce H_2O_2 again (Eq. (14)). The reactions in the 12 - 14 caused the negative effect on MB degradation. In order to test weather the addition of H_2O_2 possesses a significant effect on the degradation of MB, the Duncan test was performed. The results were shown in the Appendix 13, which clearly supported the results.

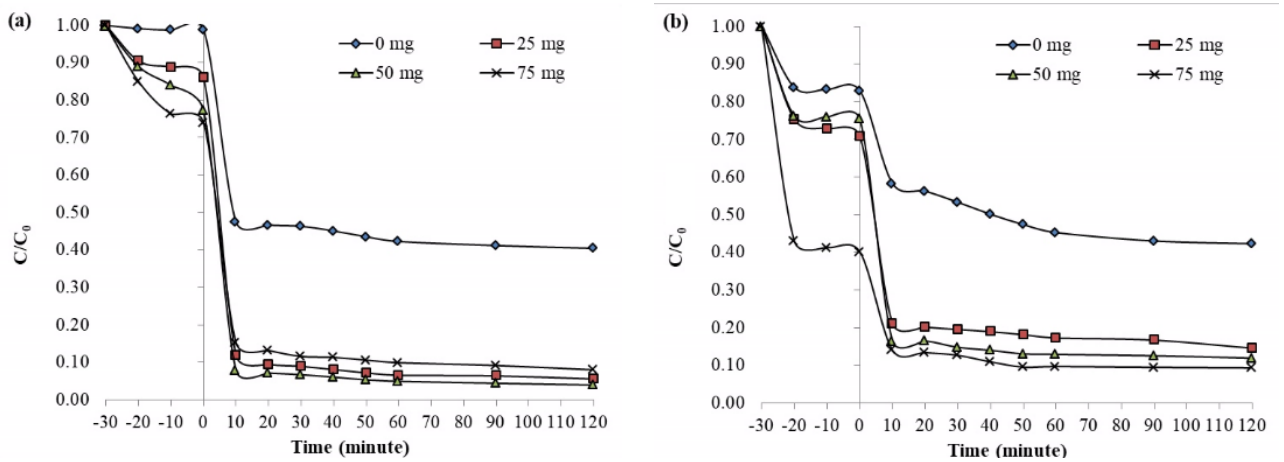

Figure 11 The curve of the relationship of time to C/C_0 ratio by the synthesized catalysts at different mass by catalyst (a) C-4/700 and (b) C-4/500. Description: C_0 MB 12.5 ppm; pH 11; volume H_2O_2 30 % 15 mL. C/C_0 = normalized concentration of MB.

A catalyst plays a crucial role in degrading MB by activating the H_2O_2 solution, leading to the production of hydroxyl radicals (OH•). A catalyst also acts as an active site where adsorption and degradation processes occur. To study the effect of catalyst concentration on the degradation of MB, the amount of C-4 catalyst was varied (0, 25, 50 and 75 mg). The results are displayed in **Figures 10(a) - 10(b)** for the catalysts C-4/700 and C-4/500, respectively. The Anova test was also conducted to assess whether the catalyst concentration

gave significantly different percent degradation. The data from Anova test can be seen in Appendix 13. The results showed that the addition of catalysts resulted in significant effect on the degradation of MB. Without the catalyst, MB removal achieved was only 59.59 ± 0.61 % after 120 min of reaction time. Following the addition of C-4/700 catalyst, the percent of degradation increased to 94.46 ± 1.44 %, 96.07 ± 0.33 % and 92.03 ± 0.31 % for the addition of catalyst as much as 25, 50 and 75 mg, respectively after 120 min of reaction time. More catalyst added means more active sites are available for a reaction to occur, thus more OH• radicals to degrade MB molecules. The degradation of MB without the presence of the C-4 catalyst could be due to the decomposition of H_2O_2 itself absorbing light to produce OH• and OH^- [46]. However, this reaction requires a longer time to occur and also produce H_2O and O_2.

The **Figure 11(a)** also indicated that the optimum mass of the catalyst was 50 mg and used to study the effect of initial MB concentration on the degradation of MB. The Duncan test in Appendix 13 was also conducted to validate the result. The addition of excess catalyst resulted in the decreased catalytic performance. Excessive catalyst can lead to agglomeration, where particles clump together, decreasing the surface area available for reaction.

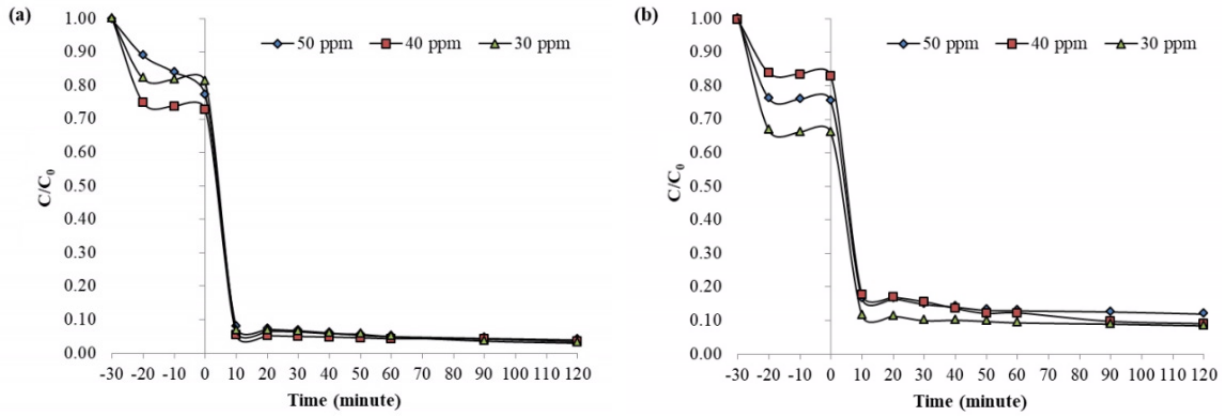

Figure 12 the curve of the relationship of time to C/C_0 ratio by the synthesized catalysts at different different C_0 MB by catalysts (a) C-4/700 and (b) C-4/500. Description: Mass of catalyst 50 mg; pH 11; volume H_2O_2 30 % 15 mL. C/C_0 = normalized concentration of MB.

The influence of initial concentration of MB on the degradation of MB was shown in **Figures 12(a) - 12(b)**. The degradation of MB for C-4/700 catalyst relatively unchanged after 120 min of reaction time. For C-4/500 catalyst, there is a significant different in the catalytic performance at 10 min of reaction time with different initial concentration of MB. In the low initial concentration (30 ppm) of MB, the catalyst was able to degrade almost 90 % of MB, whereas the degradation of MB reached only about 80 % in the medium (40 ppm) and high (50 ppm) initial concentration of MB. It is believed that the active sites of the catalyst were almost fully covered by MB molecules at 10 min of reaction time for low concentration of MB. The degradation of MB remained relatively constant after 10 min of reaction time, suggesting that the surface of the C-4/500 catalyst was fully covered by MB molecules. For the C-4/700 catalyst, the catalytic performance remained high even at high concentration of MB. After 10 min of reaction time, the catalyst successfully degraded over 90 % of MB from an initial concentration of 50 ppm. For C-4/700 catalyst, the percent degradation of MB is similar for the 3 different initial concentration of MB. However, the Anova test data (appendix 13) indicated that there are statistically significant differences between percent degradation of MB due to the C-4/700 catalyst at different initial concentration of MB.

Conclusions

The nanostructured cryptomelane-type manganese oxides have been successfully synthesized using precipitation method with simultaneous mixing of the solutions of $KMnO_4$ and glucose. The characterization of the as-synthesized manganese oxides using XRD

revealed that the pure cryptomelane phases were produced for all reactant concentration ratios. The SEM images showed that as the calcination temperature increased, nanostructured particles formed with smaller sizes. The IR spectroscopy also confirmed the presence of Mn-O bond vibrations at wave numbers 430 to 700 cm^{-1} and O-Mn-O vibrations at wave numbers 482 and 488 cm^{-1} and Raman spectroscopy further supported presence of pure cryptomelane phase at Raman shifts 184.01, 579.71 and 654.71 cm^{-1}. The concentration of reactant $KMnO_4$ and glucose greatly affect the physicochemical properties such as crystal size, morphology and AOS of Mn. The catalyst with the lowest concentration ratio (0.04/0.06) displayed the highest catalytic performance for the degradation of MB, which correlated lowest particle size and AOS of Mn. The catalytic performance of the as-synthesized cryptomelanes was optimized by varying the type of catalyst, solution pH, volume of H_2O_2, the catalyst mass and the initial concentration of MB solution. The results indicated that the molar ratio 0.04/0.06 of the catalyst was able to degrade 97.01 ± 0.33 % of MB using 30 ppm of initial concentration of MB, 15 mL H_2O_2, 50 mg of catalyst, 120 min of reaction time at pH 11.

Acknowledgements

We would like to thank all members of the research team and laboratory parties who helped in the implementation of this research. This research was funded by a grant fundas based on 0667/E5/AL.04/2024 behalf of Prof. Dr. Amir Awaluddin, M.Sc with contract number 20581/UN19.5.1.3/AL.04/2024 carried out at the University of Riau, Indonesia laboratory by the research team.

References

[1] R Yang, Y Fan, R Ye, Y Tang, X Cao, Z Yin and Z Zeng. MnO_2-based materials for environmental applications. *Advanced Materials* 2021; **33(9)**, e2004862.

[2] B Debnath, AS Roy, S Kapri and S Bhattacharyya. Efficient dye degradation catalyzed by manganese oxide nanoparticles and the role of cation valence. *ChemistrySelect* 2016; **1(14)**, 4265-4273.

[3] C Gong, X Lv, S Liu, X Chen, R Weerasooriya and Z Ding. Novel α-MnO_2/AC catalysts for heterogeneous catalytic ozonation process to remove BAA in dye wastewater. *Journal of Industrial and Engineering Chemistry* 2024; **141**, 340-350.

[4] R Anggraini, SS Siregar, A Linggawati, H Sophia and A Awaluddin. Manganosite MnO-oil palm fly ash composite for pH-dependent degradation of methylene blue. *Materials Today Proceedings* 2023; **87(9)**, 370-375.

[5] S Ching, JL Roark, N Duan and SL Suib. Sol-gel route to the tunneled manganese oxide Cryptomelane. *Chemistry of Materials* 1997; **9(3)**, 750-754.

[6] A Awaluddin, M Agustina, RR Aulia and Muhdarina. Precursor effects on the morphology and crystallinity of manganese oxides and their catalytic application for MB degradation. *AIP Conference Proceedings* 2017; **1823**, 020108.

[7] A Awaluddin, E Amiruddin, SS Saidah and R Anggraini. The catalytic activity of manganosite MnO/activated carbon for photo-degradation of synthetic dye. *E3S Web of Conferences* 2023; **481(1)**, 03007.

[8] A Awaluddin, R Zulfa, S Absus, Nurhayati, A Linggawati and SS Siregar. The enhanced catalytic activities of octahedral layer birnessite-type manganese oxide synthesized via precipitation method for the degradation of MB. *IOP Conference Series: Materials Science and Engineering* 2019; **509**, 012011.

[9] N Subramanian, B Viswanathan and TK Varadarajan. A facile morphology-controlled synthesis of potassium-containing manganese oxide nanostructures for electrochemical supercapacitor application. *RSC Adv*ances 2014; **4(1)**, 33911-33922.

[10] S Kurniati, Asleni, A Linggawati, SS Siregar and A Awaluddin. Synthesis and catalytic activities of manganese oxides prepared by precipitation method: effects of mixing modes of reactants and calcination process. *Journal of Physics: Conference Series* 2019; **1351**, 012035.

[11] S Absus, R Zulfa, A Awaluddin, S Anita, SS Siregar and Prasetya. A facile synthesis of octahedral layered birnessite-type manganese oxide (OL-1) nanostructures with tremendous catalytic activity for MB degradation. *AIP Conference Proceedings* 2018; **2049**, 020009.

[12] S Asleni, A Kurniati, A Linggawati, SS Siregar and A Awaluddin. The tremendous influence of calcination process on the phase structure and catalytic activity of precipitation-processed MnO_2. *Journal of Physics Conference Series* 2019; **1351(1)**, 012038.

[13] P Enrico. Impact of textile industry liquid waste on the environment and application of ECO printing techniques as an effort to reduce waste. *Moda* 2018; **1(1)**, 5-13.

[14] AM Wati, FW Mahatmanti, Jumaeri and AT Prasetya. Methylene blue adsorption by activated coal fly ash using microwave-assisted hydrothermal process. *Journal of Chemical Research* 2022, **18(1)**, 58-69.

[15] AB Baunsele and H Missa. Langmuir and freundlich equation test on methylene blue adsorption by using coconut fiber biosorbent. *Walisongo Journal of Chemistry* 2021; **4(2)**, 131-138.

[16] Fathoni. Utilization of technical bentonite as dye adsorbent. *UNESA Journal of Chemistry* 2016; **5(3)**, 18-22.

[17] S Hashemian, MK Ardakani and H Salehifar. Kinetics and thermodynamics of adsorption methylene blue onto tea waste/CuFe2O4 composite. *American Journal of Analytical Chemistry* 2013; **4(7)**, 1-7.

[18] AT Saputra, Y Tiandho and F Afriani. Studi kinetika pada proses elektrokoagulasi zat warna metilen biru. *Indonesian Journal of Physics Research* 2022; **3(1)**, 1-11.

[19] Maryudi, A Aktawan and S Amelia. Treatment of MB dye waste using activated charcoal and activated zeolite with fe catalyst and hydrogen peroxide oxidizer. *Journal of Chemical Research* 2021; **12(2)**, 112-120.

[20] YA Kakame, AD Wuntu and H Koleangen. Degradation and adsorption of MB dye using calcined ag-fish bone composite. *Chemistry Progress* 2018; **11(2)**, 58-62.

[21] KC He, Y Chen, Z Tang and Y Hu. Removal of heavy metal ions from aqueous solution by zeolite. *Environmental Science and Pollution Research* 2016; **23(3)**, 2778-2788.

[22] L Sun, D Hu, Z Zhang and X Deng. Oxidative degradation of MB via pds-based advanced oxidation process using natural pyrite. *International Journal of Environmental Research and Public Health* 2019; **16(23)**, 4773,

[23] YD Deng and R Zhao. Advanced oxidation processes (AOPs) in wastewater treatment. *Current Pollution Reports* 2015; **1**, 167-176.

[24] M Subkhan, A Awaluddin, Prasetya, SS Siregar and R Anggraini. Degradasi Katalitik Zat Warna Metil Jingga Menggunakan Katalis Oksida Mangan Manganosite. *Photon: Jurnal Sain Dan Kesehatan* 2018; **9(1)**, 177-183.

[25] D Yu, Y Ren, X Yu, X Fan, L Wang, R Wang, Z Zhao, K Cheng, Y Chen, Z Sojka, A Kotarba, Y Wei and J Liu. Facile synthesis of birnessite-type $K_2Mn_4O_8$ and cryptomelane-type K_2-xMn_8O_{16} catalysts and their excellent catalytic performance for soot combustion with high resistance to H_2O and SO_2. *Applied Catalysis B: Environmental* 2021; **285**, 119779.

[26] ME Becerra, AM Suarez, NP Arias and O Giraldo. Decomposition of the MB dye using layered manganese oxide materials synthesized by solid state reactions. *International Journal of Chemical Engineering* 2018; **2018**, 4902376

[27] SS Siregar and A Awaluddin. Synthesis and catalytic activity of Birnessite-Type Manganese Oxide synthesized by solvent-free method. *IOP Conference Series Materials Science and Engineering* 2018; **345(1)**, 012005.

[28] M Ghaly, SS Metwally, EA El-Sherief, EA Saad and ROA Rahman. Utilization of synthetic nano-cryptomelane for enhanced removal of cesium and cobalt ions from single and binary solutions. *Journal of Radioanalytical and Nuclear Chemistry* 2022; **331(1-3)**, 1821-1838.

[29] Y Zhou, Y Feng, H Xie, J Lu, D Ding and S Rong. Cryptomelane nanowires for highly selective self-heating photothermal synergistic catalytic oxidation of gaseous ammonia. *Applied Catalysis B: Environmental* 2023; **331**, 122668.

[30] NTH Nguyen, GT Tran, NTT Nguyen, TT Nguyen, DTC Nguyen and TV Tran. A critical review on the biosynthesis, properties, applications and future outlook of green MnO_2 nanoparticles. *Environmental Research* 2023; **231(2)**, 116262.

[31] C Stella, N Soundararajan and K Ramachandran. Structural, optical, dielectric and magnetic properties of $Mn_{1x}Co_xO_2$ nanowires. *Superlattices and Microstructures* 2014; **71**, 203-210.

[32] T Jakubek, C Hudy, J Gryboś, H Manyar and A Kotarba. Thermal transformation of birnessite (OL) towards highly active cryptomelane (OMS-2) catalyst for soot oxidation. *Catalysis Letters* 2019; **149(8)**, 2218-2225.

[33] J Hou, Y Li, L Liu, R Lu and X Zhao. Effect of giant OVD on the catalytic oxidation of OMS-2 nanorods. *Journal of Materials Chemistry A* 2013; **1(23)**, 6736-6741.

[34] Y Meng, W Song, H Huang, Z Ren, SY Chen and SL Suib. Structure-property relationship of 555 bifunctional MnO2 nanostructures: highly efficient, ultra-stable electrochemical water 556 oxidation and oxygen reduction reaction catalysts identified in alkaline media. *Journal of the American Chemical Society* 2014; **136(32)**, 11452-11464.

[35] DM Robinson, YB Go, M Mui, G Gardner, Z Zhang, DDT Mastrogiovanni, E Garfunkel, J Li, M Greenblatt, GC Dismukes. Photochemical water oxidation by crystalline polymorphs of 630 manganese oxides: structural requirements for catalysis. *Journal of the American Chemical Society* 2013; **135(9)**, 3494-3501.

[36] U Maitra, B Naidu, A Govindaraj and CNR Rao. Importance of trivalency and the eg1 632 configuration in the photocatalytic oxidation of water by Mn and Co oxides. *Proceedings of the National Academy of Sciences of the United States of America* 2013; **110(29)**, 11704-11707

[37] W Yuan, X Yang, C Liu, L Xue, W Niu, Q Yan, Y Zhu, J Han, W Guo and B Zhang. High-surface-area Co-Cu-B monolithic self-supported catalyst for efficient sodium borohydride hydrolysis. *Processes* 2024, **12(7)**, 1384.

[38] JR Frade. Kinetics of nucleation and growth. *Journal of Materials Science* 1993; **28**, 6715-6718

[39] Y Zheng, Y Shen, Y Ma, J Wang, X Wu, M Yang, M Xu and Jiao Wang. Nucleation, growth, and aggregation kinetics of KCI produced by stirred crystallization. *Applied Physics A* 2023; **129(9)**, 651.

[40] H Zhang, S Du, Y Wang and F Xue. Prevention of crystal agglomeration: Mechanisms, factors, and impact of additives. *Crystals* 2024; **14(8)**, 676.

[41] S Jia, X Wan, T Yao, S Guo, Z Gao, J Wang and J Gong. Separation performance and agglomeration behavior analysis of solution crystallization in food engineering. *Food Chemistry* 2023; **419**, 136051.

[42] LA Vijaya, K Mounika, T Jyothi and C Sailu. Effect of temperature and processing time on agglomerates prepared by spherical crystallization. *Journal of Emerging Technologies and Innovative Research* 2021; **8(5)**, d375-d383.

[43] C Yu, G, Li, L Wei, Q Fan, Q Shu and JC Yu. Fabrication, characterization of B-MnO2 microrod catalysts and their performance in rapid degradation of dyes of high concentration. *Catalysis Today* 2021; **224**, 154-162.

[44] TT Yu, KL Li, XL Guo, F Li, JM Huang and YX Zhang. Facile decolorization of methylene blue by morphology-dependence δ-MnO_2 nanosheets - modified diatomite. *Journal of Physiscs and Chemsistry of Solids* 2015; **87**, 196-202.

[45] Z Erda, Nurhayati, E Amirudin, R Anggraini, SS Siregar and A Awaluddin. Influencing parameters for degradation of MB using the catalyst bentonite supported manganosite MnO synthesized via facile, one-pot sol-gel route. *Journal of Physics: Conference Series*. 2021; **2049(1)**, 012061.

[46] S Naniwa, A Yamamoto and H Yoshida. Visible light-induced Minisci reaction through photoexcitation of surface Ti-peroxo species. *Catalysis Science & Technology* 2021; **11(10)**, 3376-3384.

[47] HJ Ciu, HZ Huang, B Yuan and ML Fu. Decolorization of RhB dye by manganese oxides: Effect of crystal type and solution pH. *Geochemical Transaction* 2015; **16(1)**, 10.